Notes

Contents

1 Important parameters **1**
- 1.1 On (unbound) hyperbolic orbits . . . 2
- 1.2 Bound binary in elliptic orbit . . . 2
- 1.3 Evolution equations of e and a . . . 3

2 Aspects of gravitational wave emission **3**
- 2.1 Multipole expansion formalism . . . 3
- 2.2 Application to binary system . . . 3
  - 2.2.1 Energy loss . . . 4
  - 2.2.2 Angular momentum loss . . . 6
  - 2.2.3 Frequency spectrum . . . 6

3 Formation of binaries through gravitational wave capture **9**

4 Dynamics affecting the binary's orbital evolution **9**
- 4.1 GW-driven inspiral of binary . . . 9
- 4.2 Disk - BBH dynamics . . . 11
  - 4.2.1 (Simplified) model of AGN . . . 11
  - 4.2.2 A little on accretion disks . . . 12
  - 4.2.3 Evolution of binary in global disk . . . 13
  - 4.2.4 Internal orbital evolution . . . 14
  - 4.2.5 Disc evolution 2 . . . 16
- 4.3 Plots . . . 18

5 Merger rate ("steady state distribution") **21**
- 5.1 Mass distributions . . . 21
- 5.2 Rate per Galaxy . . . 23
  - 5.2.1 BBH distributions within radial shell . . . 23
  - 5.2.2 Rate within radial shell . . . 24
  - 5.2.3 Merger rate for galaxy . . . 25

6 Merger rate ("Dynamical capture") **25**

Bibliography **26**

1 Important parameters

Here is a list of parameters that are used throughout the text.

- Geometrized unit system where $c = G = 1$, so that e.g. $[\mathrm{L}]_{\mathrm{SI}} = [\mathrm{T}]_{\mathrm{SI}} = [\mathrm{M}]_{\mathrm{SI}} = [\mathrm{L}]_{\mathrm{GUS}}$
- Total mass $M_{\mathrm{tot}} = m_1 + m_2$. The secondary-to-primary mass ratio is $q = \frac{m_2}{m_1}$. The symmetric mass ratio is $\eta = \frac{m_1 m_2}{M_{\mathrm{tot}}^2}$. The reduced mass is $\mu = M_{\mathrm{tot}}\eta = M_{\mathrm{tot}}\frac{q}{(1+q)^2}$.

- Distance of nearest approach (pericenter distance) r_p
- Semimajor axis $a = \frac{r_p}{1-e}$ for an elliptic orbit with eccentricity e
- The mean angular frequency (radians per unit time) is from Kepler's third law

$$\omega_{\rm orb} = \sqrt{\frac{M_{\rm tot}}{a^3}} \tag{1}$$

- Orbital period $T = 2\pi\omega_{\rm orb}^{-1}$

1.1 On (unbound) hyperbolic orbits

- Semi-major axis

$$-a = \frac{M_{\rm tot}}{v^2}$$

- Eccentricity

$$e^2 = 1 + \frac{b^2 v^4}{M_{\rm tot}^2}$$

- Pericenter distance

$$r_p = -a(e-1) = \frac{M_{\rm tot}}{v^2}\left[\left(1+\frac{b^2v^4}{M_{\rm tot}^2}\right)^{1/2} - 1\right].$$

Here b is the impact parameter. For small relative velocities v this simplifies to

$$r_p \simeq \frac{b^2v^2}{2M_{\rm tot}}\left(1 - \frac{b^2v^4}{4M_{\rm tot}^3}\right). \tag{2}$$

1.2 Bound binary in elliptic orbit

- Orbital energy of two orbiting bodies is the sum of their mutual potential energy and their total kinetic energy

$$E = M_{\rm tot}\eta\left(\frac{v^2}{2} - \frac{M_{\rm tot}}{r}\right) = -\frac{\eta M_{\rm tot}^2}{2a}. \tag{3}$$

- The absolute value of the orbital angular momentum is

$$J = \mu\sqrt{M_{\rm tot}a(1-e^2)} = \mu\omega_{\rm orb}a^2\sqrt{1-e^2}. \tag{4}$$

- Eccentricity

$$e^2 = 1 + \frac{2EL^2}{M_{\rm tot}^2\,\mu^3} = 1 + \frac{2Ev^2b^2}{M_{\rm tot}^2\,\mu}. \tag{5}$$

1.3 Evolution equations of e and a

The evolution equations of the eccentricity and semi-major axis of a bound binary are obtained by differentiating equations (3) and (5),

$$\frac{d\log a}{dt} = \frac{1}{a}\frac{da}{dt} = -\frac{\dot{E}}{E} + \frac{2\dot{M}_{\rm tot}}{M_{\rm tot}} + \frac{\dot{\eta}}{\eta}, \tag{6}$$

and

$$\frac{de}{dt} = \frac{1-e^2}{2e}\left[-\frac{2\dot{L}}{L} - \frac{\dot{E}}{E} + \frac{2\dot{M}_{\rm tot}}{M_{\rm tot}} - \frac{3\dot{\mu}}{\mu}\right]. \tag{7}$$

Under the assumption that $\dot{M}_{\rm tot} = \dot{\mu} = 0$, the last equation can be rewritten as

$$\frac{de}{dt} = \frac{a(1-e^2)}{e\mu M_{\rm tot}}\left[\dot{E} - \frac{M_{\rm tot}^{1/2}}{a^{3/2}(1-e^2)^{1/2}}\dot{L}\right]. \tag{8}$$

2 Aspects of gravitational wave emission

2.1 Multipole expansion formalism

2.2 Application to binary system

A good reference for details and derivations regarding the multipole expansion formalism of gravitational waves is [1].
In the wave zone, gravitational waves can be treated as linearised perturbations propagating on a flat background metric. This background metric can be characterized by a Minkowskiian coordinate system whose origin coincides with the source. In this coordinate frame the transverse and traceless part of the metric perturbation has then the form

$$h_{ij}^{TT} = \frac{1}{r}A_{ij}(t-r,\theta,\phi), \tag{9}$$

where A_{ij} is a traceless and transverse tensor varying in the wave zone rapidly in the radial direction but slowly in the transverse direction. The angular dependence of the radiation field A_{ij} can be decomposed into spin-2 tensor spherical harmonics. Because A_{ij} is traceless and transverse, it can contain only the TT harmonics $\mathbf{T}^{\mathrm{E2},lm}$ and $\mathbf{T}^{\mathrm{B2},lm}$. For $l=0$ and $l=1$ there are no TT harmonics. Therefore the radiation field has the form

$$h_{ij}^{TT} = \frac{1}{r}\sum_{l=2}^{\infty}\sum_{m=-l}^{l}\left[{}^{(l)}I^{lm}(t-r)\,T_{ij}^{\mathrm{E2},lm} + {}^{(l)}S^{lm}(t-r)\,T_{ij}^{\mathrm{B2},lm}\right]. \tag{10}$$

The expansion coefficients ${}^{(l)}I^{lm}$ and ${}^{(l)}S^{lm}$ are the lth time derivative of the mass multipole moments I^{lm} and the current multipole moments S^{lm}. I^{lm} is given by

$$I^{lm} = \frac{16\pi}{(2l+1)!!}\left(\frac{(l+1)(l+2)}{2l(l-1)}\right)^{1/2}\mathcal{G}_{A_l}\mathcal{Y}^{lm*}_{A_l}, \tag{11}$$

and S^{lm} has a similar expression which we however don't need throughout this work.

2.2.1 Energy loss

In the multipole formalism the total radiated power is given by

$$P = \frac{dE}{dt} = \frac{1}{32\pi} \sum_{l=2}^{\infty} \sum_{m=-l}^{l} \left\langle |^{(l+1)}I^{lm}|^2 + |^{(l+1)}S^{lm}|^2 \right\rangle . \tag{12}$$

We are interested only in the mass quadrupole radiation, *i.e.* we consider only contributions to leading order in $(v/c)^2$. This amounts to neglecting contributions arising from S^{lm} and to neglecting contribution from I^{lm} for $l > 2$. If the source is non-relativistic and has a negligible self-gravity, we can express $\mathcal{G}$ in terms of the Newtonian mass density ρ

$$\mathcal{G}_{a_1 a_2} = \int d^3x \, \rho \, x_{a_1} x_{a_2}; \tag{13}$$

this expression is also known as the second mass moment. Then

$$I^{2m} = \frac{16\pi}{5\sqrt{3}} \int d^3x \, \rho \, \mathcal{Y}^{2m*}_{a_1 a_2} \, x_{a_1} x_{a_2} \tag{14}$$

$$\equiv \frac{16\pi}{5\sqrt{3}} \int d^3x \, \rho \, r^2 Y^{2m*}. \tag{15}$$

We choose a coordinate system whose origin coincides with the center of mass of the system and we let the binary lie in the $\theta = \pi/2$-plane. The two masses can then be specified by $(r_1 \cos\phi, r_1 \sin\phi)$ and $(-r_2 \cos\phi, -r_2 \sin\phi)$ with $r_i = \frac{\mu r}{m_i}$. The problem is equivalent to a one body problem of a reduces mass orbiting about the total mass located at the center of mass. Thus

$$I^{2m} = \frac{16\pi}{5\sqrt{3}} \left[m_1 \frac{\mu^2 r^2}{m_1^2} Y^{2m*}\left(\frac{\pi}{2}, \phi\right) + m_2 \frac{\mu^2 r^2}{m_2^2} Y^{2m*}\left(\frac{\pi}{2}, \phi + \pi\right) \right]. \tag{16}$$

The $Y^{2\pm1*}\left(\frac{\pi}{2}, \phi\right)$ terms vanish, so we get $Y^{2m*}\left(\frac{\pi}{2}, \phi\right) = Y^{2m*}\left(\frac{\pi}{2}, \phi + \pi\right)$. Thus

$$I^{2m} = \frac{16\pi}{5\sqrt{3}} \mu r^2 \, Y^{2m*}\left(\frac{\pi}{2}, \phi\right). \tag{17}$$

In the quadrupole approximation the power radiated by the system reduces from expression (12) to

$$P = \frac{1}{32\pi} \sum_{m=-2}^{2} \left\langle |^{(3)}I^{2m}|^2 \right\rangle \tag{18}$$

The orbit equations

$$r = \frac{a(1-e^2)}{1 + e\cos\phi}, \tag{19}$$

$$\frac{d\phi}{dt} = \frac{[M_{\rm tot} a(1-e^2)]^{1/2}}{r^2} = \left(\frac{M_{\rm tot}}{a^3}\right)^{1/2} \frac{(1 + e\cos\phi)^2}{(1-e^2)^{3/2}}. \tag{20}$$

allow the calculation of the time derivatives of I^{2m}. Employing these identities, the third time derivatives of I^{2m} read

$$
\begin{aligned}
{}^{(3)}I^{20} &= \left(\frac{64\pi}{15}\right)^{1/2} \frac{\mu M_{\rm tot}^{3/2}}{[r_p(1+e)]^{5/2}} \left(1+e\cos\phi\right)^2 e\sin\phi, \\
{}^{(3)}I^{2-2} &= \left(\frac{32\pi}{5}\right)^{1/2} \frac{\mu M_{\rm tot}^{3/2}}{[r_p(1+e)]^{5/2}} \left(1+e\cos\phi\right)^2 \left[-e\sin\phi - 4i(1+e\cos\phi)\right] e^{2i\phi}, \\
{}^{(3)}I^{22} &= {}^{(3)}I^{2-2*}.
\end{aligned}
$$

The radiated power as a function of ϕ along the orbit is then

$$
P(\phi) = \frac{8}{15}\frac{\mu^2 M_{\rm tot}^3}{[r_p(1+e)]^5} \left(1+e\cos\phi\right)^4 \left[e^2\sin^2\phi + 12(1+e\cos\phi)^2\right]. \tag{21}
$$

Hyperbolic orbit $e \geq 1$**:** The asymptotes of the hyperbolic orbit are given by $\cos\psi = -1/e$. Thus the total energy released by a binary on an hyperbolic orbit is

$$
\begin{aligned}
E &= \int_{\psi}^{-\psi} P(\phi)\frac{dt}{d\phi}\,d\phi \\
&= \frac{8}{15}\frac{\eta^2 M_{\rm tot}^{9/2}}{(r(1+e))^{7/2}} \int_{\psi}^{-\psi} d\phi \left(1+e\cos\phi\right)^2 \left[e^2\sin^2\phi + 12(1+e\cos\phi)^2\right] \\
&= \frac{\eta^2 M_{\rm tot}^{9/2}}{180\, r_p^{7/2}(1+e)^{7/2}} [(12(96+292e^2+37e^4)\phi + 48e(96+73e^2)\sin\phi \\
&+ 24e^2(71+12e^2)\sin 2\phi + 368e^3\sin 3\phi + 33e^4\sin 4\phi]_{-\psi}^{\psi}
\end{aligned}
$$

For a parabolic orbit, $e = 1$, this becomes

$$
E = \frac{85\pi}{12\sqrt{2}}\frac{\eta^2 M_{\rm tot}^{9/2}}{r_p^{7/2}}. \tag{22}
$$

Closed orbit $e < 1$**:** The average of $P(\phi)$ over one orbital period T is

$$
\begin{aligned}
\frac{dE}{dt} = P &= \frac{\omega}{2\pi}\int_0^{2\pi} P(\phi)\frac{dt}{d\phi}\,d\phi \\
&= \frac{8}{15}\frac{1}{(1-e^2)^{7/2}}\frac{\mu^2 M_{\rm tot}^3}{a^5}\int_0^{2\pi}\frac{d\phi}{2\pi}(1+e\cos\phi)^2\left[e^2\sin^2\phi + 12(1+e\cos\phi)^2\right].
\end{aligned}
$$

The integral evaluates to $12 + \frac{73}{2}e^2 + \frac{37}{8}e^4$. Therefore we arrive at

$$
\frac{dE}{dt} = \frac{32}{5}\frac{\mu^2 M_{\rm tot}^3}{a^5}\frac{1}{(1-e^2)^{7/2}}\left(1 + \frac{73}{24}e^2 + \frac{37}{96}e^4\right). \tag{23}
$$

2.2.2 Angular momentum loss

In the multipole expansion formalism, the change in angular momentum of a system due to gravitational wave emission is given by

$$\frac{dL_j}{dt} = \sum_{l=2}^{\infty} \frac{(l+1)(l+2)}{(l-1)l!(2l+1)!!} \left\langle \epsilon_{jpq}{}^{(l)}\mathcal{G}_{pA_{l-1}}{}^{(l+1)}\mathcal{G}_{qA_{l-1}} \right\rangle \tag{24}$$

$$+ \sum_{l=2}^{\infty} \frac{4l^2(l+2)}{(l-1)(l+1)!(2l+1)!!} \left\langle \epsilon_{jpq}{}^{(l)}\mathcal{S}_{pA_{l-1}}{}^{(l+1)}\mathcal{S}_{qA_{l-1}} \right\rangle . \tag{25}$$

In the quadrupole approximation this reduces to

$$\frac{dL_j}{dt} = \frac{2}{5} \left\langle \epsilon_{jpq}{}^{(2)}\mathcal{G}_{pa}{}^{(3)}\mathcal{G}_{qa} \right\rangle . \tag{26}$$

We want to determine the GW-induced angular momentum loss of a binary on a Keplerian orbit. To this end we choose a coordinate system such that the orbits lies in the $(x, y)-$plane; then we can set $L = L_z$. Therefore

$$\frac{dL}{dt} = \frac{2}{5} \left\langle {}^{(2)}\mathcal{G}_{1a}{}^{(3)}\mathcal{G}_{2a} - {}^{(2)}\mathcal{G}_{2a}{}^{(3)}\mathcal{G}_{1a} \right\rangle .$$

Upon integration by parts

$$\frac{dL}{dt} = \frac{4}{5} \left\langle {}^{(2)}\mathcal{G}_{12} \left({}^{(3)}\mathcal{G}_{11} - {}^{(3)}\mathcal{G}_{22} \right) \right\rangle .$$

The second mass moments in our chosen coordinate frame are given by

$$\mathcal{G}_{a_1a_2} = \mu r^2 \begin{bmatrix} \cos^2\phi & \cos\phi\sin\phi \\ \cos\phi\sin\phi & \sin^2\phi \end{bmatrix}_{a_1a_2} . \tag{27}$$

FILL IN CALCULATION

The angular momentum change averaged over one orbital period is then

$$\frac{dL}{dt} = \frac{32}{5} \frac{\mu^2 M^{5/2}}{a^{7/2}} \frac{1}{(1-e^2)^2} \left(1 + \frac{7}{8}e^2 \right) . \tag{28}$$

2.2.3 Frequency spectrum

In this section we compute, for a Keplerian elliptic orbit, the frequency spectrum of the radiated power $\frac{dP}{d\omega}$. For this we perform a Fourier decomposition of the Keplerian motion and of its second mass moment.

We parametrize the Keplerian orbit in the following form

$$x(\beta) = a(\cos u - e), \tag{29}$$

$$y(\beta) = b \sin u. \tag{30}$$

Here a is the semi-major axis and b is the semi-minor axis of the orbit. The eccentric anomaly u is defined by the Kepler equation $u - e\sin u = \omega(t - t_0) \equiv \beta$, the time t_0 being an integration constant chosen such that $x(-\beta) = x(\beta)$ and

$y(\beta) = -y(-\beta)$. The solution of the Kepler equation can be given as a Fourier expansion involving Bessel functions. To see this we make the ansatz

$$y(\beta)\frac{e}{b} = u - \beta = e\sin u = \sum_{n=1}^{\infty} a_n \sin(n\beta), \tag{31}$$

where the coefficients are given by

$$a_m = \frac{2}{\pi}\int_0^{\pi} d\beta\,(u-\beta)\sin(m\beta). \tag{32}$$

We now compute

$$\begin{aligned} a_m &= -\frac{2e}{\pi m}\int_0^{\pi} d\beta\ \sin u\,\frac{d}{d\beta}\cos(m\beta) \\ &= \frac{2e}{\pi m}\int_0^{\pi} du\,\frac{d\sin u}{du}\ \cos(m\beta) \\ &= \frac{2e}{\pi m}\int_0^{\pi} du\ \cos u\ \cos(mu - me\sin u) \\ &= \frac{e}{m}\int_0^{\pi}\frac{du}{\pi}\ \left[\cos(u(m-1) - me\sin u) + \cos(u(m+1) - me\sin u)\right]. \end{aligned}$$

By using the integral representation of the Bessel function

$$J_n(z) = \int_0^{\pi}\frac{du}{\pi}\cos(nu - z\sin u) \tag{33}$$

we arrive at

$$a_m = \frac{e}{m}\left[J_{m-1}(me) + J_{m+1}(me)\right]. \tag{34}$$

Using the Bessel functions identity

$$J_{n-1}(z) + J_{n+1}(z) = \frac{2n}{z}J_n(z), \tag{35}$$

this result can be rewritten as

$$a_m = \frac{2}{m}J_m(me). \tag{36}$$

Similarly we write $\frac{x(\beta)}{a} = \cos u - e = b_0 + \sum_{n=1}^{\infty} b_n\cos(n\beta)$ and find for the corresponding expansion coefficients

$$a_0 = -\frac{3}{2}e, \tag{37}$$

$$a_m = \frac{2}{m}J'_m(me). \tag{38}$$

Next we compute the Fourier expansion of $x^2(\beta)$, $y^2(\beta)$ and $x(\beta)y(\beta)$. We can again write

$$y^2(\beta) = A_0 + \sum_{n=1}^{\infty} A_n\cos(n\beta), \tag{39}$$

$$x^2(\beta) = B_0 + \sum_{n=1}^{\infty} B_n\cos(n\beta), \tag{40}$$

$$y(\beta)x(\beta) = \sum_{n=1}^{\infty} C_n\sin(n\beta), \tag{41}$$

together with

$$A_m = \frac{2}{\pi}\int_0^\pi d\beta\, y^2(\beta)\cos(m\beta), \tag{42}$$

$$B_m = \frac{2}{\pi}\int_0^\pi d\beta\, x^2(\beta)\cos(m\beta), \tag{43}$$

$$C_m = \frac{2}{\pi}\int_0^\pi d\beta\, x(\beta)y(\beta)\sin(m\beta). \tag{44}$$

Similar to the calculation of a_n we obtain

$$A_m = \frac{b^2}{m}\left[J_{m+2}(me) - J_{m-2}(me)\right], \tag{45}$$

$$B_m = \frac{a^2}{m}\left[J_{m-2}(me) - J_{m+2}(me) - 4eJ'_m(me)\right], \tag{46}$$

$$A_m = \frac{ba}{m}\left[J_{m+2}(me) + J_{m-2}(me) - 2J_m(me)\right], \tag{47}$$

along with $A_0 = \frac{1}{2}$ and $B_0 = \frac{1+4e^2}{2}$.

Likewise we expand the second mass moment (13) as

$$\mathcal{G}_{a_1a_2} = \mu\sum_{n=0}^{\infty}\begin{bmatrix} B_n\cos(n\beta) & C_n\sin(n\beta) & 0 \\ C_n\sin(n\beta) & A_n\cos(n\beta) & 0 \\ 0 & 0 & 0 \end{bmatrix}_{a_1a_2} \equiv \sum_{n=0}^{\infty}\mathcal{G}^{(n)}_{a_1a_2}. \tag{48}$$

The emitted power in the quadrupole approximation is obtained from the formulae (11) and (18)

$$P = \frac{1}{10\sqrt{3}}\sum_{m=-2}^{2}\left\langle \left|{}^{(3)}\mathcal{G}_{a_1a_2}\left(\mathcal{Y}^{2m}_{a_1a_2}\right)^*\right|^2\right\rangle. \tag{49}$$

Since $= 0$ different harmonics don't contribute in the power spectrum. Hence we have $P = \sum_{n=1}^{\infty} P_n$ and the power radiated in the n-th harmonics is

$$P_n = \frac{1}{10\sqrt{3}}\sum_{m=-2}^{2}\left\langle \left|{}^{(3)}\mathcal{G}^{(n)}_{a_1a_2}\left(\mathcal{Y}^{2m}_{a_1a_2}\right)^*\right|^2\right\rangle, \tag{50}$$

together with

$${}^{(3)}\mathcal{G}^{(n)}_{a_1a_2} = \mu(\omega n)^3\begin{bmatrix} B_n\sin(n\beta) & -C_n\sin(n\beta) & 0 \\ -C_n\sin(n\beta) & A_n\sin(n\beta) & 0 \\ 0 & 0 & 0 \end{bmatrix}_{a_1a_2}. \tag{51}$$

The explicit form of the STF tensors $\mathcal{Y}^{2m}_{a_1a_2}$ is given by

$$\mathcal{Y}^{22}_{a_1a_2} = \left(\frac{15}{32\pi}\right)^{1/2} \begin{pmatrix} 1 & i & 0 \\ i & -1 & 0 \\ 0 & 0 & 0 \end{pmatrix}_{a_1a_2}, \tag{52}$$

$$\mathcal{Y}^{21}_{a_1a_2} = -\left(\frac{15}{32\pi}\right)^{1/2} \begin{pmatrix} 0 & 0 & 1 \\ 0 & 0 & i \\ 1 & i & 0 \end{pmatrix}_{a_1a_2}, \tag{53}$$

$$\mathcal{Y}^{20}_{a_1a_2} = \left(\frac{5}{16\pi}\right)^{1/2} \begin{pmatrix} -1 & 0 & 0 \\ 0 & -1 & 0 \\ 0 & 0 & 2 \end{pmatrix}_{a_1a_2}, \tag{54}$$

together with $\mathcal{Y}^{2-m}_{a_1a_2} = (-1)^m \left(\mathcal{Y}^{2m}_{a_1a_2}\right)^*$.

3 Formation of binaries through gravitational wave capture

When two parabolic black holes have a near encounter, they may release sufficient energy through GWs to form a bound binary. The initial energy of two non-interacting BHs is $E_{\rm ini} = \frac{\mu v^2}{2}$. If δE denotes the emitted energy though GWs, the final energy of the binary system is $E_{\rm fin} = E_{\rm ini} - \delta E$. For there to be a bound binary, $E_{\rm fin}$ must be negative. This criterion gives a constraint for the formation of a bound binary. Accordingly, the maximal impact parameter of two colliding BHs with relative velocity v to form a binary is

$$b_{\rm max} = M_{\rm tot} \left(\frac{340\pi}{3}\right)^{1/7} \left(\frac{\eta}{v^9}\right)^{1/7}, \tag{55}$$

where equation (22) was expanded to first order in the relative velocity v. Substituting $b_{\rm max}$ in equation (2) the corresponding maximum pericenter distance reads

$$r_{p,\rm max} = 2^{-3/7} M_{\rm tot} \left(\frac{85\pi}{3}\right)^{2/7} v^2 \left(\frac{t}{v^9}\right)^{2/7} \left[1 - 2^{-10/7} \left(\frac{85\pi}{3}\right)^{2/7} v^4 \left(\frac{t}{v^9}\right)^{2/7}\right] \tag{56}$$

4 Dynamics affecting the binary's orbital evolution

The hardening time $\frac{a}{\dot{a}}$ is the time a binary spends at each semimajor-axis a.

4.1 GW-driven inspiral of binary

Once a binary is formed its orbital parameters are affected due to the release of GWs.

Substituting the energy loss equation (23) into the evolution equation (6) one finds the GW driven evolution of the semi-major axis

$$\frac{da}{dt} = -\frac{64}{5}\frac{\mu M_{\rm tot}^2}{a^3}\frac{1}{(1-e^2)^{7/2}}\left(1+\frac{73}{24}e^2+\frac{37}{96}e^4\right). \tag{57}$$

Substituting both (23) and (28) into the evolution equation (8) one finds the GW driven evolution of the orbit eccentricity

$$\frac{de}{dt} = -\frac{304}{15}\frac{\mu M_{\rm tot}^2}{a^4}\frac{e}{(1-e^2)^{5/2}}\left(1+\frac{121}{304}e^2\right). \tag{58}$$

Combining equations (57) and (58) gives

$$\frac{da}{de} = \frac{12}{19}a\frac{1+(73/24)e^2+(37/96)e^4}{e(1-e^2)\left(1+e^2\frac{121}{304}\right)}. \tag{59}$$

The solution of the differential equation (59) is

$$a(e) = c_0\,\frac{e^{12/19}}{1-e^2}\left(1+\frac{121}{304}e^2\right)^{870/2299}, \tag{60}$$

where c_0 depends on the initial semi-major axis a_0 and the initial orbital eccentricity e_0. By requiring $a(e_0) = a_0$ we can set

$$c_0 = a_0\left(1-e_0^2\right)e_0^{-12/19}\left(1+\frac{121}{304}e_0^2\right)^{-\frac{870}{2299}}.$$

From the orbit equation (1) we find that the orbital frequency is related to the eccentricity by

$$\frac{\omega}{\omega_0} = \left[\left(\frac{e}{e_0}\right)^{\frac{12}{19}}\frac{1-e_0^2}{1-e^2}\left(\frac{1+\frac{121}{304}e^2}{1+\frac{121}{304}e_0^2}\right)^{\frac{870}{2299}}\right]^{-3/2}, \tag{61}$$

with the initial orbital frequency $\omega_0 = \sqrt{\frac{M}{a_0^3}}$.

To find the time to coalescence τ we can integrate the inverse to equation (58) by requiring that $e(\tau) = 0$ (at coalescence the eccentricity e goes to zero). The lifetime is thus given by the integral

$$\tau = \frac{15}{304}\frac{1}{\mu M_{\rm tot}^2}\int_0^{e_0} de\, a^4\frac{(1-e^2)^{5/2}}{e}\left(1+\frac{121}{304}e^2\right)^{-1}. \tag{62}$$

We now simplify this expression for an initial parabolic orbit. We write the last equation using equation (60) and note that the integral is dominated by e near 1, thus giving

$$\tau = a_0^4\frac{15}{304}\frac{1}{\mu M_{\rm tot}^2}\left(1-e_0^2\right)^4\int_0^{e_0} de\,\frac{(1-e^2)^{5/2}}{(1-e^2)^4}\left(1+\frac{121}{304}\right)^{-1} \tag{63}$$

$$= a_0^4\frac{15}{425}\frac{1}{\mu M_{\rm tot}^2}\left(1-e_0^2\right)^4\int_0^{e_0} de\,(1-e^2)^{-3/2} \tag{64}$$

$$\approx a_0^4\frac{15}{425}\frac{1}{\mu M_{\rm tot}^2}\frac{\left(1-e_0^2\right)^4}{(1-e_0^2)^{1/2}} = a_0^4\frac{3}{85}\frac{1}{\mu M_{\rm tot}^2}\left(1-e_0^2\right)^{7/2}. \tag{65}$$

As initial semi-major axis a_0 and initial eccentricity e_0 for the bound binary we use the expressions (3) and (5). The time to merger is thus

$$\tau = \left(\frac{\eta M_{\rm tot}^2}{2E_{\rm fin}}\right)^4 \frac{3}{85}\frac{1}{\mu M_{\rm tot}^2}\left(\frac{2E_{\rm fin}v^2b^2}{M_{\rm tot}^2\,\mu}\right)^{7/2} \tag{66}$$

$$= \frac{3\sqrt{2}}{170}\frac{1}{E_{\rm fin}^{1/2}M_{\rm tot}}\frac{\eta^4}{\mu^{9/2}}v^7b^7. \tag{67}$$

As the merger time depends on v to the seventh power, we can ignore the contribution of the kinetic part of the final energy $E_{\rm fin}$ and thus use for $E_{\rm fin}$ the expression (22). In this approximation, and upon expressing r_p in δE with its parametrized form (2), the merger time reads

$$\tau = \frac{3}{170}\sqrt{\frac{3}{85\pi}}\frac{(bv)^{21/2}}{\eta^{3/2}M_{\rm tot}^{19/2}}. \tag{68}$$

4.2 Disk - BBH dynamics

The interaction between the binary system and the gaseous disk in which it is embedded is complicated and several mechanisms are at play.
At some point, the tidal torques exerted by the binary onto the disc are sufficiently high to repel gas away from the binary, thus clearing a cavity around the binary. Furthermore, the binary may then be surrounded by a circumbinary disc which affects the orbital evolution of the central binary. The disc-binary interaction drives the binary ultimately into the phase of GWs-driven inspiral, where loss of orbital energy and angular momentum is due to the emission of gravitational waves.

4.2.1 (Simplified) model of AGN

The equation for hydrostatic equilibrium in the vertical direction for a geometrically thin disk in a central gravitational potential is

$$\frac{dp}{dz} = -\rho\frac{Mz}{r^3}, \tag{69}$$

where $p(r,z)$ and $\rho(r,z)$ are the pressure and mass density at radius r and height z. We assume the disk to be isothermal in the vertical direction, yielding $c_s^2 = \frac{p}{\rho}$, where c_s is the sound speed (independent of z). Then we obtain for the mass density

$$\rho = \rho_0 e^{-\frac{z^2}{2h^2}}, \tag{70}$$

with the density at the equatorial plane ρ_0 and with the disk scale height

$$h = \frac{c_s r^{3/2}}{M^{1/2}} = \frac{c_s}{\Omega}. \tag{71}$$

The total mass enclosed within a radius r is denoted by $M(r)$ and is related to the surface density $\Sigma(r)$ through $\frac{dM(r)}{dr} = 2\pi r\Sigma(r)$. In the AGN model

outlined in [2], the disk mass $M(r)$ is set to $2\sigma^2 r$, where σ stands for the velocity dispersion of the gas. The associated surface density is then

$$\Sigma(r) = \frac{\sigma^2}{\pi r}. \tag{72}$$

Furthermore, the following relations are imposed to the disk data

$$\frac{f_g}{2^{3/2}} = \frac{h}{r} = \frac{1}{\sqrt{2}}\frac{c_s}{\sigma}, \tag{73}$$

where $f_g = \frac{\Sigma}{\Sigma_g}$ is the total surface density Σ divided by the gas surface density Σ_g. The last relation ensures that ...

4.2.2 A little on accretion disks

Continuity equation for accretion disks Suppose that a gaseous disk has surface density $\Sigma(r)$ and radial velocity $v_\phi = r\Omega(r)) = \frac{M}{r}$. The structure and the evolution of gaseous disks can be deduced from the continuity equation

$$2\pi r\frac{\partial \Sigma}{\partial t} = \frac{\partial \dot{M}}{\partial r}, \tag{74}$$

and from angular momentum conservation

$$\frac{\partial(\Omega r^2)}{\partial r}\dot{M} = \frac{\partial}{\partial r}(T_{\text{visc}}). \tag{75}$$

Combining equations (74) and (75) gives an evolution equation for the surface density Σ,

$$\frac{\partial \Sigma}{\partial t} = \frac{1}{2\pi r}\frac{\partial}{\partial r}\left[\left(\frac{\partial(\Omega r^2)}{\partial r}\right)^{-1}\frac{\partial(T_{\text{visc}})}{\partial r}\right]. \tag{76}$$

We can incorporate external effects interacting with the disk into the viscous evolution equation of the disk. If the disk experiences an external torque per unit mass $\tilde{T}_{\text{ext}}$, we modify the surface density evolution in the following form

$$\frac{\partial \Sigma}{\partial t} = \frac{1}{2\pi r}\frac{\partial}{\partial r}\left[\left(\frac{\partial(\Omega r^2)}{\partial r}\right)^{-1}\frac{\partial(T_{\text{visc}})}{\partial r} + \frac{4\pi\Sigma\tilde{T}_{\text{ext}}}{\Omega}\right] \tag{77}$$

$$= \frac{1}{2\pi r}\frac{\partial}{\partial r}\left[\left(\frac{\partial(\Omega r^2)}{\partial r}\right)^{-1}\frac{\partial(T_{\text{visc}} + T_{\text{ext}})}{\partial r}\right], \tag{78}$$

defining $\frac{\partial T_{\text{ext}}}{\partial r} = 8\pi\Sigma\tilde{T}_{\text{ext}}r$.

Viscous Torque in the Disc Because the angular velocity of the accretion disk varies with radius, a viscous torque is acting on the gas. This torque represents the amount of angular momentum crossing the disk circumference at radius r per unit time due to the action of viscosity. The shear stress is $\tau = \rho(r)\nu r\frac{d\Omega}{dr}$, where ν is the dynamical viscosity and $\rho(r)$ the mass density. This leads to a viscous torque between two neighbouring disk annuli at radius r

$$T_{\text{visc}} = 2\pi r\int dz\, r\tau = 2\pi\nu\Sigma(r)r^3\frac{d\Omega}{dr}, \tag{79}$$

where $\Sigma(r) = \int dz\, \rho(r)$ is the surface density of the disk. By employing the Keplerian orbital frequency it follows that the torque is

$$T_{\text{visc}} = -3\pi\nu\Sigma(r)r^2\Omega(r). \tag{80}$$

One may employ the $\alpha-$disk prescription to parametrize the dynamical viscosity in the case for a thin accretion disk as $\nu = \alpha c_s^2(r)\Omega(r)^{-1}$, where $c_s(r)$ is the local gas sound speed and $0 \leq \alpha \leq 1$ is a dimensionless constant. Substituting this value for ν into the expression for T_{visc} gives

$$T_{\text{visc}} = -3\pi\alpha c_s^2(r)\Sigma(r)r^2. \tag{81}$$

Note that this torque is negative, resulting in an outward transfer of angular momentum.

4.2.3 Evolution of binary in global disk

Several simulations suggest that a binary system carves an annular gap or even a cavity into the global disk. The presence of such a gap may help to both understand how the binary migrates towards the central disk mass and how its orbital parameters evolve.

Criterion for gap-opening in disk In order for the binary to open a gap in the disk, the gap-opening torque must be greater than the gap-closing torque. Crida et al. [3] derived a semi-analytical criterion for gap-opening based on the balance between pressure, gravitational and viscous torques for a compact object on a fixed circular orbit around a central mass M_*. Adapting their work to binary systems orbiting circularly around a central mass may not be justified. The parameters of the binary orbit are expected to complicate the mechanisms of gap-opening. However, deriving a formula which additionally takes into account the internal angular momentum of the binary, its semi-major-axis and its eccentricity seems without resorting to numerical simulations out of reach. Such simulations have been performed and are discussed in section (4.2.4) and suggest that the simplified criterion for gap-opening may nevertheless be useful. The gap-opening criterion is given by $g \lesssim 1$, where

$$g = \frac{3}{4}\frac{h}{R_{\text{Hill}}} + \frac{50\nu_b}{qr_b^2\Omega_b}. \tag{82}$$

Here r_b is the distance from the center of mass of the binary to the central mass M_*, h denotes the thickness of the disk, $R_{\text{Hill}} = r_b\left(\frac{M_b}{3M_*}\right)^{1/3}$ is the Hill radius of the binary, $\Omega_b = \sqrt{\frac{M_b+M_*}{r_b^3}}$ is the angular orbital frequency of the binary-central mass system and ν_b is the dynamical viscosity of the disk at the binary orbit. Writing the disk viscosity according to the α-disk model, the inequality becomes

$$g = \frac{3}{4}\frac{h}{R_{\text{Hill}}} + \frac{50\alpha h^2\Omega_r}{qr_b^2\Omega_b}, \tag{83}$$

where again $h = c_s/\Omega_r = c_s\sqrt{\frac{r^3}{M_*}}$ is the scale height of the disk.

For $\alpha = 0.01$ and a disk scale height varying from 10^{-3} at 0.01pc to 10^{-2} at 1pc, table (1) lists some approximate disc radii in parsec up to which a gap may be opened (horizontal: Central mass M_* in solar masses, vertical: Binary mass M_b in solar masses)

	3×10^5	3×10^6	3×10^7
10	1.75	0.06	$\ll 0.01$
20	4.71	0.17	< 0.01
30	8.38	0.31	0.01
40	> 10	0.47	0.02
50	> 10	0.63	0.02
100	> 10	1.74	0.06
150	> 10	3.16	0.11
200	> 10	4.68	0.17

Table 1: Approximate disk radii in parsec up to which a binary system may open a gap in its embedded disk.

4.2.4 Internal orbital evolution

Numerical simulations suggest the presence of a depleted cavity inside of which the binary resides (Condition: the binary mass ratio q gets closer to unity). The gas orbiting around this cavity is referred to as the circumbinary disk (CBD). The evolution of the semi-major axis and of the orbital eccentricity are driven by tidal and viscous interaction between the binary and the CBD. As we will see this results in a loss of the binary's orbital angular momentum, a increase in its eccentricity and its faster inspiral.

Orbital parameters We thus now assume that a central cavity is surrounded by a CBD. For simplicity we assume that neither the primary nor the secondary have their own disks. We aim to relate the viscous angular momentum flux in the inner region of the disk to the orbital evolution of the binary.
Numerical simulations suggest that the size of the central cavity extends to about twice the semi-major axis of the binary orbit, $r_{\rm in} = 2a$. We suppose that the cavity is coupled to dynamical changes in the semi-major axis, meaning that if the semi-major axis is changed, the cavity size is changed accordingly. Tidal torques from the binary are expected to act significantly only on a narrow annulus at the inner edge of the CBD and are thus assumed to be zero outside of some cutoff radius r_Λ. Thus the effect of the binary torque on the disk evolution can be accounted for via equation (78) by imposing suitable boundary conditions at the inner edge of the disk. From equation (78) we can thus deduce

$$\left(\frac{\partial(\Omega r^2)}{\partial r}\right)\dot{M} = \frac{\partial(T_{\rm visc})}{\partial r} + \left(\frac{\partial(\Omega r^2)}{\partial r}\right)\frac{4\pi\Sigma\tilde{T}_{\rm ext}}{\Omega}. \tag{84}$$

Integrating from r_b to r_Λ we obtain (check this at some point)

$$T_{\rm visc}(r_\Lambda) = 8\pi\int_{r_b}^{r_\Lambda} dr\, r\Sigma\tilde{T}_{\rm ext} - 2\int_{r_b}^{r_\Lambda} dr\, r\Omega\dot{M}; \tag{85}$$

we have set $T_{\rm visc}(r_b) = 0$ because of the clean gap assumption. The first integral on the right hand side is the total torque the binary exerts on the disk. As long

as the evolution of the binary is driven predominantly by the tidal coupling to the disk (and not due to the gravitational wave emission) conservation of angular momentum guarantees that it is equal to $-\dot{J}_b$, the change of angular momentum of the binary. In the right integral on the right side we can write

$$\dot{M} = 2\pi\Sigma r v_r = 3\pi\Sigma\nu = 3\pi\Sigma\alpha c_s^2/\Omega. \tag{86}$$

Because of the clean gap assumption, the disk surface density Σ is zero for $r < r_{in}$. Then we approximate the integral by

$$\begin{aligned}\Delta &\equiv -6\pi\alpha c_s^2\Sigma(r_{in})\int_{r_{in}}^{r_\Lambda} dr\, r \\ &= -3\pi\alpha c_s^2\Sigma(r_{in})\left[r_\Lambda^2 - r_{in}^2\right] \\ &\approx -3\pi\alpha c_s^2\Sigma(r_{in})\delta r_{in},\end{aligned}$$

where the disk density in the small radial annulus $[r_{in}, r_\Lambda]$ around the cavity edge we set to $\Sigma(r_{in})$ since $r_\Lambda - r_{\rm in} = \delta/2 \ll r_{\rm in}$ and since we have no model to resolve the surface density of the CBD down to this scale.

Therefore we may suppose that $T_{\rm visc}(r_{\rm in}) = -\dot{J}_b - \Delta$. Recall that $r_{in} = 2a$, so the viscous torque (81) reads $T_{\rm visc}(2a) = 12\pi\alpha c_s^2\Sigma(2a)a^2$. As this term is a few order of magnitudes higher than Δ, we may neglect Δ henceforward. The change in the binary energy is related to its change in angular momentum through the orbital frequency, $\dot{E}_b = \Omega_b\dot{J}_b$. From the evolution equation (6) for the semi-major axis of the binary orbit and the binary energy $E_b = -\frac{\Omega_b J_b}{2\sqrt{1-e^2}}$ it follows therefore

$$\frac{\dot{a}}{a} = -\frac{\dot{E}_b}{E_b} = -\frac{T_{\rm visc}(r_{\rm in})}{J_b}2\sqrt{1-e^2} \tag{87}$$

$$= -2\frac{T_{\rm visc}(r_{\rm in})}{\mu\Omega_b a^2}, \tag{88}$$

where the last equation follows by substituting the orbital angular momentum (4). Substituting the explicit formula for the viscous torque results in

$$\frac{\dot{a}}{a} = -\frac{24\pi\alpha c_s^2\Sigma(2a)}{\mu\Omega_b}. \tag{89}$$

Similarly we obtain for the evolution of the eccentricity

$$\frac{e\dot{e}}{1-e^2} = \left(\frac{1}{\sqrt{1-e^2}} - 1\right)\frac{T_{\rm visc}(r_{\rm in})}{\mu\Omega_b a^2} \tag{90}$$

$$= \left(\frac{1}{\sqrt{1-e^2}} - 1\right)\frac{12\pi\alpha c_s^2\Sigma(2a)}{\mu\Omega_b}. \tag{91}$$

What values of α, Σ and c_s of the CBD should be used? Baruteau et al. [4] use the same values as those of the global AGN disk. It is argued that the quantities taken at the inner edge of the CBD should not differ significantly from the quantities taken at the outer edge of the CBD and there those quantities should not differ from their values in the global disk around the central mass M_*. We use the same assumption due to lack of a better alternative, realizing that it may however not be justified.

4.2.5 Disc evolution 2

If the tidal interaction with the binary presents a strong barrier for the gas inflow, then mass accretion onto the binary is vanishingly small. This is the case when the mass ratio is close to unity. For low values of q, tidal torques do not have to completely stop the mass inflow.
In the following we present a model for the migration of the secondary BH which allows to estimate the mass accretion. To this end, we use a (semi-)analytical expression for the tidal torque on the disk from the presence of the secondary mass (in the previous section we ignored the detailed form of the tidal torque). For a Keplerian disk the surface density evolution (78) is governed by the equation

$$\frac{\partial \Sigma}{\partial t} = \frac{1}{r}\frac{\partial}{\partial r}\left[3r^{1/2}\frac{\partial}{\partial r}\left(\nu\Sigma r^{1/2}\right) - \frac{2r^{3/2}\Sigma\tilde{T}_{\rm tid}}{M_1^{1/2}}\right], \tag{92}$$

where we incorporated the tidal effect of the disk-secondary interaction through the injection rate of angular momentum per unit mass $\tilde{T}_{\rm tid}$.
Goldreich and Tremaine in [5] calculated amplitudes of the torque produced by the individual azimuthal Fourier harmonics of the secondary potential. Assumptions: low q, and use epicycle approximation (nearly circular orbits). Chandrasekhar 156! get expressions of Goldstein. Their result for the radial density torque is

$$\frac{dT}{dr} = \mathrm{sign}(r-a)\frac{\kappa^2 r\Sigma}{2^3A^4}\frac{M_2^2}{(a-r)^4}\left\{\frac{2\Omega}{\kappa}K_0\left(\frac{\kappa}{2|A|}\right) + K_1\left(\frac{\kappa}{2|A|}\right)\right\}^2. \tag{93}$$

For a Keplerian orbit this simplifies to

$$\frac{dT}{dr} = \mathrm{sign}(r-a)\frac{r\Sigma}{\Omega^2}\frac{M_2^2}{(a-r)^4}\frac{32}{81}\left\{2K_0\left(\frac{2}{3}\right) + K_1\left(\frac{2}{3}\right)\right\}^2 \tag{94}$$

$$\approx \mathrm{sign}(r-a)f\frac{r\Sigma}{\Omega^2}\frac{M_2^2}{(a-r)^4} = \mathrm{sign}(r-a)\Sigma f q^2 M_1\frac{r^4}{(a-r)^4}, \tag{95}$$

with $f \approx 2.5$.
The (unperturbed, not taking epicyle into account) angular momentum of the secondary is $L = M_2 a^2\Omega$. The torque exerted at each ring annulus T_r changes the angular momentum of the secondary according to (angular momentum exchange between the disk and the secondary may cause secular orbital evolution of the secondary)

$$\frac{dL}{dt} = -T_r. \tag{96}$$

Thus we find the change in orbital separation due to the torque acting at radius r (using $\kappa(a) = 2\Omega(a)$)

$$\begin{aligned}\dot{a} &= -\frac{1}{2a\Omega(a)M_2}T_r \\ &= \frac{1}{2a\Omega(a)M_2}\left(\mathrm{sign}(a-r)\Sigma f q^2 M_1\frac{r^4}{(a-r)^4}\right)\end{aligned}$$

Finally ($M_r = 2\pi\Sigma r dr$):

$$\frac{\dot{a}}{a} = 0.798\frac{M_2 M_r}{M_1^2}\Omega\left(\frac{a}{a-r}\right)^4 \text{sign}(a-r)$$

Summing all contributions yields

$$\begin{aligned}\frac{\dot{a}}{a} &= 0.798\frac{M_2}{M_1^2}\int_{R_{in}}^{R_{out}} M_r\Omega\left(\frac{a}{a-r}\right)^4 \text{sign}(a-r) \\ &= 2\pi\times 0.798\frac{M_2}{M_1^2}\sqrt{M_1}a^4\left[\int_{R_{in}}^{a'} dr\Sigma\frac{r^{-1/2}}{(a-r)^4} - \int_{a''}^{R_{out}} dr\Sigma\frac{r^{-1/2}}{(a-r)^4}\right].\end{aligned}$$

Tentatively, pulling out Σ and setting $a' = a-\delta$ and $a'' = a+\delta$

$$\begin{aligned}\frac{\dot{a}}{a} &= 2\pi\times 0.798\frac{M_2}{M_1^2}\sqrt{M_1}a^4\Sigma\ \times \\ &\times\left[\left[\frac{5\tanh^{-1}(\frac{\sqrt{r}}{\sqrt{a}})}{8a^{7/2}} + \frac{\sqrt{r}(33a^2-40ar+15r^2)}{24a^3(a-r)^3}\right]_{r=R_{in}}^{r=a'} - \left[\frac{5\tanh^{-1}(\frac{\sqrt{r}}{\sqrt{a}})}{8a^{7/2}} + \frac{\sqrt{r}(33a^2-40ar+15r^2)}{24a^3(a-r)^3}\right]_{r=a''}^{r=R_{ou}}\right.\end{aligned} \tag{97}$$

2nd try:
Summing all contributions yields

$$\begin{aligned}\frac{\dot{a}}{a} &= 0.798\frac{M_2}{M_1^2}\int_{R_{in}}^{R_{out}} M_r\Omega\left(\frac{a}{a-r}\right)^4 \text{sign}(a-r) \\ &= 2\pi\times 0.798\frac{M_2}{M_1^2}\Omega a^4\left[\int_{R_{in}}^{a'} dr\Sigma\frac{r}{(a-r)^4} - \int_{a''}^{R_{out}} dr\Sigma\frac{r}{(a-r)^4}\right].\end{aligned}$$

Tentatively, pulling out Σ and setting $a' = a-\delta$ and $a'' = a+\delta$

$$\begin{aligned}\frac{\dot{a}}{a} &= 2\pi\times 0.798\frac{M_2}{M_1^2}\sqrt{M_1}a^4\Sigma\ \times \\ &\times\left[\left[\frac{a-3r}{6(r-a)^3}\right]_{r=R_{in}}^{r=a'} - \left[\frac{a-3r}{6(r-a)^3}\right]_{r=a''}^{r=R_{out}}\right].\end{aligned} \tag{98}$$

mass accretion

$$\begin{aligned}\dot{M} &= 2\pi\Sigma r v_r \\ &= 2\pi\Sigma\nu\frac{3}{2}.\end{aligned}$$

Contribution to semi-major axis evolution.

$$\begin{aligned}\dot{a} &= \frac{2\dot{M}a}{M} \\ &= \frac{6\pi\Sigma\alpha c_s^2 a}{M\Omega}.\end{aligned}$$

4.3 Plots

One may add to the above disk-driven orbital evolution equations the corresponding GW driven evolution equations (57) and (58). This coupled system of differential equations can be integrated numerically. Among the various ordinary differential equations solvers in Matlab, the ode23tb function performed best. This solver is designed for solving stiff ordinary differential equations. Indeed, during the latest stages of inspiral, the solution displays much variation within a short time interval.

As expected, at most values of a the disk-binary interaction dominates the GW emission which reduces the GW-driven merger time by several orders of magnitudes. The disk-binary dynamics reduces the binary's semi-major axis while at the same time increasing the orbit's eccentricity. At a critical semi-major axis (where $\dot{a}_{\rm GW} = \dot{a}_{\rm CDB}$) the binary decouples from the disk and evolves (until coalescence) thereafter predominately under the emission of GWs.

Figure (1) shows a comparison between the purely GW-driven merger times (blue) and those where in addition disk interactions are taken into account (green). The red curve shows the remaining time to coalescence after the binary has decoupled from the gas and GW-emission has taken over. The system parameters can be seen in the graphic; as noted earlier the CBD values are taken to be those of the global disk.

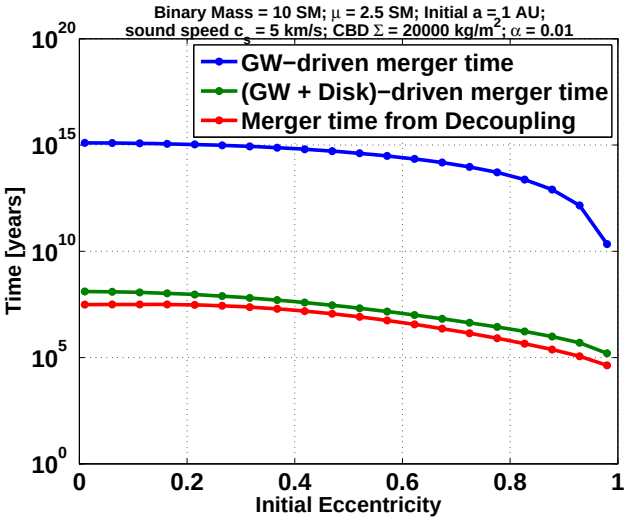

Figure 1: Merger times as a function of the initial binary eccentricity. The blue curve represents the merger times resulting from GW-driven decay, the green one resulting from both GW emission and disk-binary interaction. The red curve shows the time for which the binary evolution is dominated by GWs emission.

Figure (2) displays the AGN profile as described in section (4.2.1). The velocity dispersion σ was set to $\sigma = 200\,\mathrm{km/s}$ and $f_g = 0.05$.

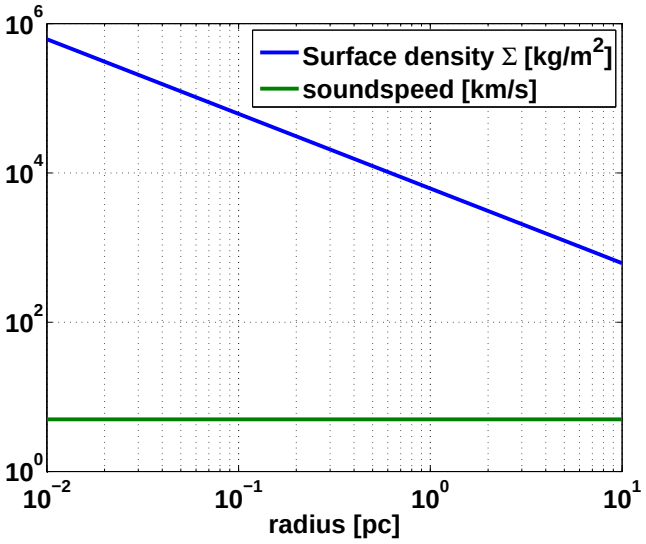

Figure 2: Key parameters as a function of the radius of the AGN disk.

In figure (3) the merger times for a binary are plotted as a function of the binary's location in an AGN disk having the profile of figure (2).

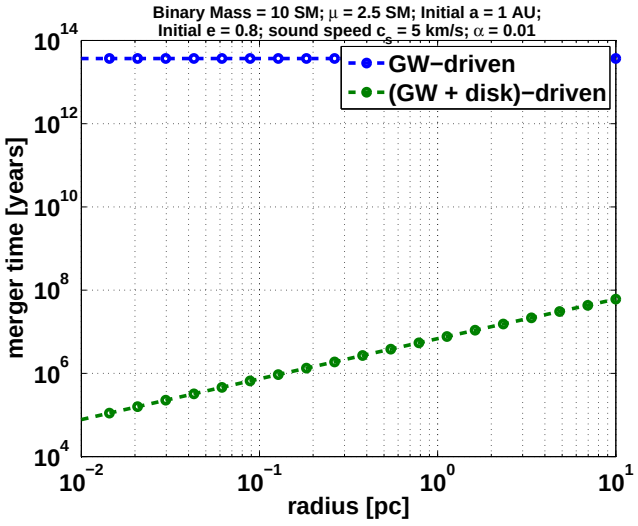

Figure 3: The merger times for a binary as a function of its location in the AGN disk (blue for GW-driven and green for (GW+gas)-driven).

In figure (4) the merger times for a binary are plotted as a function of the initial binary semi-major axis a_0 for two different location of the binary in the AGN disk (blue at 0.01 pc, green at 10 pc). As a_0 increases, the merger time decreases.

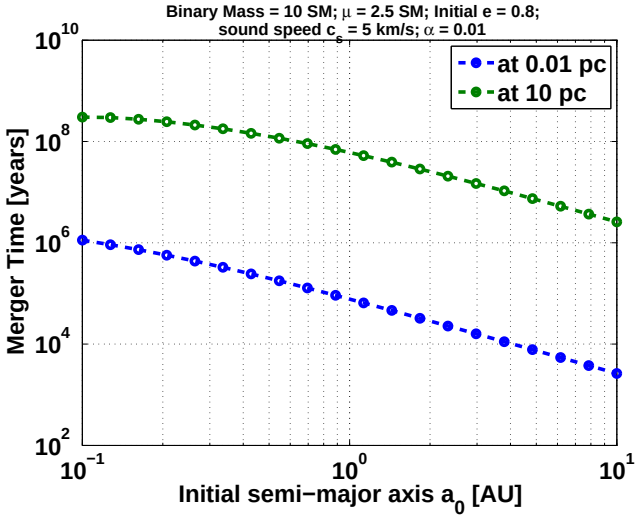

Figure 4: The merger times for a binary as a function of its initial semi-major axis. The two curves stand for two different binary locations in the background disk.

Figure (5) shows, as a function of the global disk radius, the lowest initial semi-major axis for which the merger time is less than 10^6 years (blue) or less than 10^8 years (green). *I.e.* for values a_0 lying above the curve, the merger time is less than 10^6 or 10^8 years.

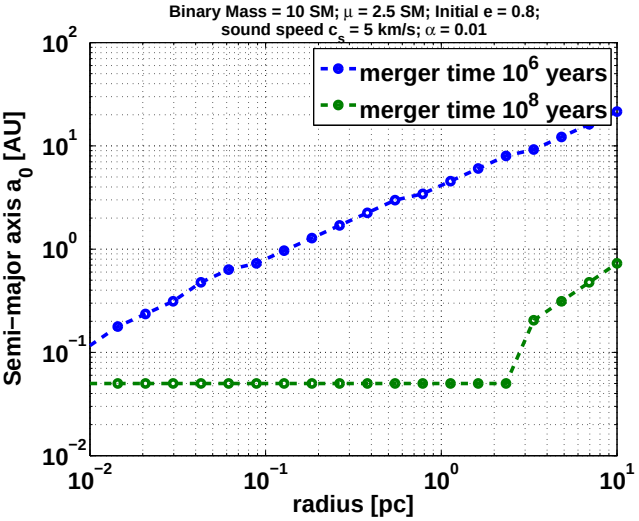

Figure 5: The curves show the smallest initial binary semi-major axis a_0 for which the merger time is shorter that 10^6 and 10^8 years.

5 Merger rate ("steady state distribution")

Here some vocabulary:

- Galactic merger rates (number of coalescences per unit time within a galaxy)
- Local merger rate density (number of coalescences per unit time per unit volume in the local Universe, i.e. around redshift=0)
- Binary fraction $f_b = \frac{N_b}{N_{\rm sBH}}$

In this section we calculate the merger rate given a fixed radial mass distribution (thus not taking into account changes in the mass distribution due to e.g. dynamical friction).
We start with an initial stellar distribution. We assume that all stars above a critical mass have evolved into black holes. We further assume that a fraction $f_b = \frac{2N_b}{N_{\rm BH}}$ of the total number of BHs formed BH binaries.

5.1 Mass distributions

Stellar distribution The initial stellar mass distribution seems to follow a multiple power-law function [6]

$$f_{\rm IMF}(m) = \begin{cases} k_0 \left(\frac{m}{M_\odot}\right)^{-0.3} & \text{if } m < 0.08 M_\odot \\ k_1 \left(\frac{m}{M_\odot}\right)^{-1.3} & \text{if } 0.08 M_\odot < m < 0.5 M_\odot \\ k_2 \left(\frac{m}{M_\odot}\right)^{-2.3} & \text{if } m > 0.5 M_\odot \end{cases}, \tag{99}$$

with normalization parameters $k_0, k_1 = 0.08 k_0$ and $k_2 = 0.04 k_0$. The normalization is taken such that $N_{\rm s,tot} = \int_{m_{\rm s,min}}^{m_{\rm s,max}} dm f_{\rm IMF}(m)$ and accordingly the parameter k_0 is

$$k_0 = \frac{N_{\rm s,tot}}{M_\odot} \Bigg/ \left[0.56 - \frac{1}{0.7}\left(\frac{m_{\rm s,min}}{M_\odot}\right)^{0.7} - \frac{0.04}{1.3}\left(\frac{m_{\rm s,max}}{M_\odot}\right)^{-1.3}\right]. \tag{100}$$

The total stellar mass is

$$M_* = \int_{m_{\rm s,min}}^{m_{\rm s,max}} dm\, m f_{\rm IMF} \tag{101}$$

$$= k_0 M_\odot^2 \left[0.22 - \frac{1}{1.7}\left(\frac{m_{\rm s,min}}{M_\odot}\right)^{1.7} - \frac{0.04}{0.3}\left(\frac{m_{\rm s,max}}{M_\odot}\right)^{-0.3}\right]. \tag{102}$$

We adopt the "Nuker law" parametrization ([7]) for the stellar density profile $\rho_*(r)$

$$\rho_*(r) \propto \left(\frac{r_b}{r}\right)^\gamma \left[1 + \left(\frac{r}{r_b}\right)^\alpha\right]^{\frac{\gamma-\beta}{\alpha}}, \tag{103}$$

We simplify this profile by using its asymptomatic slopes,

$$\rho_*(r) = \begin{cases} \rho_0 \left(\frac{r}{r_b}\right)^{-\gamma} & \text{if } r \le r_b \\ \rho_0 \left(\frac{r}{r_b}\right)^{-\beta} & \text{if } r > r_b \end{cases}; \tag{104}$$

the parameter α would parameterize the transition between the inner cusp and the outer power law. The break radius r_b is approximately on the order of the radius of influence of the SMBH ([8]), characterized as $r_b = M_{\rm SMBH}/\sigma_*^2$ (σ_* is the stellar dispersion). The normalization parameter ρ_0 can be expressed as (we only consider models with $\beta > 3$)

$$\rho_0 = \frac{M_*}{4\pi r_b^3}\left(\frac{1}{3-\gamma} - \frac{1}{3-\beta}\right)^{-1}. \tag{105}$$

BH distribution If we assume that every star heavier than $m_{\rm cr}$ evolved into a BH, the total initial number of BHs is

$$N = \int_{m_{\rm s,cr}}^{m_{\rm s,max}} dm\, f_{\rm IMF} \tag{106}$$

$$= k_0 M_\odot \left[0.56 - \frac{1}{0.7}\left(\frac{m_{\rm s,cr}}{M_\odot}\right)^{0.7} - \frac{0.04}{1.3}\left(\frac{m_{\rm s,max}}{M_\odot}\right)^{-1.3}\right] \tag{107}$$

$$= kM_*, \tag{108}$$

where we defined

$$k = \frac{1}{M_\odot}\frac{\left[0.56 - \frac{1}{0.7}\left(\frac{m_{\rm s,cr}}{M_\odot}\right)^{0.7} - \frac{0.04}{1.3}\left(\frac{m_{\rm s,max}}{M_\odot}\right)^{-1.3}\right]}{\left[0.22 - \frac{1}{1.7}\left(\frac{m_{\rm s,min}}{M_\odot}\right)^{1.7} - \frac{0.04}{0.3}\left(\frac{m_{\rm s,max}}{M_\odot}\right)^{-0.3}\right]}. \tag{109}$$

The total mass of all BHs is

$$M_{\rm BH} = \int_{m_{\rm s,cr}}^{m_{\rm s,max}} dm\, m\, f_{\rm IMF}. \tag{110}$$

The BH mass distribution is denoted as $f_{\rm BH}(m)$ and is normalized such that $\int dm f_{\rm BH}(m) = 1$. We adopt a Salpeter mass function for the BH distribution

$$f_{\rm BH}(m) = \xi_0 m^{-2.35}; \tag{111}$$

the normalization parameter ξ_0 is then

$$\xi_0 = -\frac{1.35}{m_{\rm BH,max}^{-1.35} - m_{\rm BH,min}^{-1.35}}. \tag{112}$$

If $N(r)$ denotes the total number of BHs inside some radius r, the number dN of BHs lying inside r with masses between m and $m + dm$ is

$$dN = N(r) f_{\rm BH}(m) dm \tag{113}$$

$$= kM_*(r) f_{\rm BH}(m) dm, \tag{114}$$

where $M_*(r)$ is the total stellar mass inside radius r ($M_*(\infty) \equiv M_*$). Note that for the last equality we assumed that the mass distribution of the BHs is independent of the radius at which they reside (an assumption that may not be justified). We can write dN in the following form

$$dN = dm\, k\, f_{\rm BH}(m) \int_0^r dr\, \rho_*(r) 4\pi r^2, \tag{115}$$

and this yields finally

$$\frac{dN}{dm} = \begin{cases} k\, f_{\rm BH}(m)\, \frac{4\pi\rho_0}{3-\gamma} r_b^{\gamma} r^{3-\gamma} & \text{if } r \le r_b \\ k\, f_{\rm BH}(m)\, 4\pi\rho_0 r_b^3 \left[\frac{1}{3-\gamma} + \frac{1}{3-\beta}\left[\left(\frac{r}{r_b}\right)^{3-\beta} - 1\right]\right] & \text{if } r > r_b \end{cases}. \quad (116)$$

The number of BHs with masses between m and $m+dm$ in a radial shell from radius r to $r+dr$ is accordingly

$$\begin{cases} dm\, k\, f_{\rm BH}(m)\, \frac{4\pi\rho_0}{3-\gamma} r_b^{\gamma} \left[(r+dr)^{3-\gamma} - r^{3-\gamma}\right] & \text{if } r \le r_b \\ dm\, k\, f_{\rm BH}(m)\, \frac{4\pi\rho_0}{3-\beta} r_b^3 \left[\left(\frac{r+dr}{r_b}\right)^{3-\beta} - \left(\frac{r}{r_b}\right)^{3-\beta}\right] & \text{if } r > r_b \end{cases}. \quad (117)$$

Recall also that the total number of BHs in a radial shell from radius r to $r+dr$ is

$$\begin{cases} k\, \frac{4\pi\rho_0}{3-\gamma} r_b^{\gamma} \left[(r+dr)^{3-\gamma} - r^{3-\gamma}\right] & \text{if } r \le r_b \\ k\, \frac{4\pi\rho_0}{3-\beta} r_b^3 \left[\left(\frac{r+dr}{r_b}\right)^{3-\beta} - \left(\frac{r}{r_b}\right)^{3-\beta}\right] & \text{if } r > r_b \end{cases}. \quad (118)$$

5.2 Rate per Galaxy

To determine the merger rate per galaxy, we add up the contributions from different radial shells. To this end, we partition the disk into $\mathcal{I}_r$ intervals (we assume that the disk around the SMBH is truncated at 10 pc). The number of BHs within each radial shell $[i\Delta r, (i+1)\Delta r]$, where $\Delta r = 10{\rm pc}/|\mathcal{I}_r|$ is obtained from equation (118)

$$N_{r,i} = \begin{cases} k\, \frac{4\pi\rho_0}{3-\gamma} r_b^{\gamma} \left[((i+1)\Delta r)^{3-\gamma} - (i\Delta r)^{3-\gamma}\right] & \text{if } (i+1)\Delta r \le r_b \\ k\, \frac{4\pi\rho_0}{3-\beta} r_b^3 \left[\left(\frac{(i+1)\Delta r}{r_b}\right)^{3-\beta} - \left(\frac{i\Delta r}{r_b}\right)^{3-\beta}\right] & \text{if } i\Delta r > r_b \end{cases}. \quad (119)$$

The average radius within each radial shell is

$$r_i = (i+0.5)\Delta r. \quad (120)$$

5.2.1 BBH distributions within radial shell

For the moment we assume for simplicity a binary fraction of unity, *i.e.* the number of binaries is $N/2$, where N is the total number of BHs.
Within each radial shell we assume independent primary mass, mass ratio, orbital separation and eccentricity distributions. The following distributions refer to a single radial shell $[r, r+dr]$.

Primary mass distribution We adopt the IMF of Salpeter for the primary mass distribution. Thus, in a radial shell $[r, r+dr]$, two times the number of binaries with primary mass between m and $m+dm$ is given by equation (117).

Secondary mass distribution The secondary mass distribution is determined by the distribution of the mass ratio q, assumed to follow a uniform distribution ([9],[10])

$$f(q) = \mu, \quad (121)$$

where μ is a constant and $0.1 \leq q \leq 1$. The normalization $\mu \int_{0.1}^{1} dq = \frac{1}{2} N_r$ determines μ; N_r is the total number of BHs in the shell $[r, r+dr]$, see equation (119).

Orbital separation distribution The distribution of the initial orbital separation a_0 is assumed to be logarithmically flat ([9],[10])

$$f(a_0) = \chi_0 / a_0, \tag{122}$$

between the limits 0.01 AU and 500 AU. Normalizations gives $\chi_0 = \frac{N_r}{2 \log 50000}$.

Orbital eccentricity distribution We choose the distribution of the initial orbital eccentricity e_0 to follow a thermal distribution

$$f(e_0) = \varsigma_0 e_0, \tag{123}$$

between the limits 0 and 1. Normalization gives $\varsigma_0 = N_r$.

5.2.2 Rate within radial shell

In this section we determine the merger rate for a radial shell $[r, r+dr]$. In what follows, we partition the distribution functions x into discrete intervals indexed by $\mathcal{I}_x$.

Primary mass The number of primary BHs within the mass bin $[m_{\rm BH,min} + i\Delta M, M_{\rm min} + (i+1)\Delta M]$, where $\Delta M = (m_{\rm BH,max} - m_{\rm BH,min})/|\mathcal{I}_M|$ and $i \in \mathcal{I}_M$, is obtained by integrating equation (117)

$$\begin{aligned} N_{M,i} = \frac{4\pi k \rho_0 \xi_0}{1.35} \left[(m_{\rm BH,min} + i\Delta M)^{-1.35} - (m_{\rm BH,min} + (i+1)\Delta M)^{-1.35} \right] \times \\ \times \begin{cases} \frac{1}{3-\gamma} r_b^{\gamma} \left[(r+dr)^{3-\gamma} - r^{3-\gamma} \right] & \text{if } r \leq r_b \\ \frac{1}{3-\beta} r_b^{3} \left[\left(\frac{r+dr}{r_b} \right)^{3-\beta} - \left(\frac{r}{r_b} \right)^{3-\beta} \right] & \text{if } r > r_b \end{cases}. \end{aligned} \tag{124}$$

The average mass within this mass bin is

$$M_i = \frac{1.35}{0.35} \frac{\left[(m_{\rm BH,min} + i\Delta M)^{-0.35} - (m_{\rm BH,min} + (i+1)\Delta M)^{-0.35} \right]}{\left[(m_{\rm BH,min} + i\Delta M)^{-1.35} - (m_{\rm BH,min} + (i+1)\Delta M)^{-1.35} \right]}. \tag{125}$$

Mass ratio The number of BBH within the mass ratio bin $[0.1 + i\Delta q, 0.1 + (i+1)\Delta q]$, where $\Delta q = 0.9/|\mathcal{I}_q|$ and $i \in \mathcal{I}_q$, is

$$N_{q,i} = \frac{10}{18} N_r \Delta q. \tag{126}$$

The average mass ratio within this mass ratio bin is

$$q_i = (i + 0.5)\Delta q + 0.1. \tag{127}$$

Orbital separation The number of BBH within the orbital separation bin $[0.01\text{AU}+i\Delta a, 0.01\text{AU}+(i+1)\Delta a]$, where $\Delta a = 499.99\text{AU}/|\mathcal{I}_{a_0}|$ and $i \in \mathcal{I}_{a_0}$, is

$$N_{a_0,i} = \chi_0 \log\left(\frac{0.01\text{AU} + (i+1)\Delta a}{0.01\text{AU} + i\Delta a}\right). \tag{128}$$

The average a_0 within this bin is

$$a_{0_i} = \frac{\Delta a}{\log\left(\frac{0.01\text{AU}+(i+1)\Delta a}{0.01\text{AU}+i\Delta a}\right)}. \tag{129}$$

Orbital eccentricity The number of BBH within the eccentricity bin $[i\Delta e_0, (i+1)\Delta e_0]$, where $\Delta e_0 = 1/|\mathcal{I}_{e_0}|$ and $i \in \mathcal{I}_{e_0}$, is

$$N_{e_0,i} = \varsigma_0 \, (i+0.5) \, (\Delta e_0)^2. \tag{130}$$

The average e_0 within this bin is

$$e_{0_i} = \frac{((i+1)\Delta e_0)^3 - (i\Delta e_0)^3}{3\,(i+0.5)\,(\Delta e_0)^2}. \tag{131}$$

Merger rate for a radial shell The total merger rate resulting from a radial shell is

$$\mathcal{R}_r = N_r \sum_\alpha \frac{N_\alpha}{N_r^4} \frac{1}{\tau_{\text{merger},\alpha}} \tag{132}$$

where the sum goes over all $\alpha \in \mathcal{I}_M \times \mathcal{I}_q \times \mathcal{I}_{a_0} \times \mathcal{I}_{e_0}$. Note that $N_\alpha = N_{\alpha_1} N_{\alpha_2} N_{\alpha_3} N_{\alpha_4}$.

5.2.3 Merger rate for galaxy

We set the model parameters to the fiducial values $M_{\text{SMBH}} = 1 \times 10^6 M_\odot, \gamma = 1.5; \beta = 3.2; \sigma_* = 30$ km/s; $m_{\text{s,max}} = 50000 M_\odot$; $m_{\text{s,min}} = 0.01 M_\odot$; $m_{\text{s,cr}} = 5 M_\odot$; $m_{\text{BH,max}} = 50 M_\odot$; $m_{\text{BH,min}} = 5 M_\odot$; $N_{\text{s,tot}} = 20000$; we use the disk model of section (4.2) and use partitions $|\mathcal{I}_r| = 20$ and $|\mathcal{I}_M| = |\mathcal{I}_q| = |\mathcal{I}_{a_0}| = |\mathcal{I}_{e_0}| = 2$. The galactic merger rate is then obtained by summing up the rate (132) for each shell. We obtain a rate of $\mathcal{R} = 0.02 \, \frac{1}{\text{year}}$. The rate is most sensitive to the total number of initial stars $N_{\text{s,tot}}$. Note that in the calculation we assumed that all BHs paired up to binaries, which is clearly not justified.

6 Merger rate ("Dynamical capture")

Gaussian velocity distribution.

References

1. Thorne, K. S. Multipole expansions of gravitational radiation. *Rev. Mod. Phys.* **52,** 299–339 (2 1980).
2. Thompson, T. A., Quataert, E. & Murray, N. Radiation Pressure–supported Starburst Disks and Active Galactic Nucleus Fueling. *The Astrophysical Journal* **630,** 167–185 (2005).
3. Crida, A., Morbidelli, A. & Masset, F. On the width and shape of gaps in protoplanetary disks. *Icarus* **181,** 587 –604. ISSN: 0019-1035 (2006).
4. Baruteau, C., Cuadra, J. & Lin, D. N. C. BINARIES MIGRATING IN A GASEOUS DISK: WHERE ARE THE GALACTIC CENTER BINARIES? *The Astrophysical Journal* **726,** 28 (2010).
5. Goldreich, P. & Tremaine, S. Disk-satellite interactions. *The Astrophysical Journal* **241,** 425–441 (Oct. 1980).
6. Kroupa, P. On the variation of the initial mass function. *Monthly Notices of the Royal Astronomical Society* **322,** 231–246 (2001).
7. Lauer, T. R. *et al.* The Centers of Early-Type Galaxies with HST.I.An Observational Survey. *The Astrophysical Journal* **110,** 2622 (Dec. 1995).
8. Schödel, R. *et al.* The distribution of stars around the Milky Way´s central black hole - II. Diffuse light from sub-giants and dwarfs. *A&A* **609,** A27 (2018).
9. Tout, C. A., Hurley, J. R. & Pols, O. R. Evolution of binary stars and the effect of tides on binary populations. *Monthly Notices of the Royal Astronomical Society* **329,** 897–928. ISSN: 0035-8711 (Feb. 2002).
10. Ablimit, I. & Maeda, K. Monte Carlo Population Synthesis on Massive Star Binaries: Astrophysical Implications for Gravitational-wave Sources. *The Astrophysical Journal* **866,** 151 (2018).